LA-UR-14-27648
Approved for public release; distribution is unlimited.

Title: High Temperature Mechanical Properties, Fractography and Synchrotron Studies of ATF clad materials from the UCSB-NSUF Irradiations.

Author(s): Saleh, Tarik A.
Maloy, Stuart Andrew
Romero, Tobias J.
Sprouster, David
Ecker, Lynne

Intended for: Report

Issued: 2015-02-23 (rev.1)

High Temperature Mechanical Properties, Fractography and Synchrotron Studies of ATF Clad Materials from the UCSB-NSUF Irradiations

M3FT-14LA0202131: Perform characterization on LWR-irradiated ATF clad materials

Tarik Saleh, Stuart Maloy, Tobias Romero Los Alamos National Laboratory
David Sprouster, Lynne Ecker Brookhaven National Laboratory

Introduction

A variety of tensile samples of Ferritic and Oxide Dispersion Strengthened (ODS or nanostructured ferritic) steels were placed the ATR reactor over 2 years achieving doses of roughly 4- 6 dpa at temperatures of roughly 290°C. Samples were shipped to Wing 9 in the CMR facility at Los Alamos National Laboratory and imaged then tested in tension. This report summarizes the room temperature tensile tests, the elevated temperature tensile tests (300°C) and fractography and reduction of area calculations on those samples. Additionally small samples were cut from the undeformed grip section of these tensile samples and sent to the NSLS synchrotron for high energy X-ray analysis, initial results will be described here.

Specimens

The full ATR NSUF-UCSB shipment contained a variety of samples, details of composition and sample type and general irradiation condition can be found in the report "Irradiation Test Plan for the ATR National Scientific User Facility – University of California Santa Barbara" INL document ID: PLN-2996. This report will only cover the subset of tensile samples received from this shipment, all of which have roughly 4-6dpa at an irradiation temperature of roughly 290°C. There were 56 total irradiated tensile samples across 13 different materials (Table 1). Control Samples were available for most material types. A detailed list of samples, material type and ID number can be seen in Appendix A. Samples were nominally of the standard S-1 tensile geometry (Figure 1), but were 0.020" thick and most specimens did not have the hole in the center of the grip section. A number of the F82H-IEA specimens had holes or notches in the gauge section for testing different stress states, these specimens were not tested as they need digital image correlation 2-d strain measurement techniques to assess the deformation.
Table 2 displays the calculated irradiation temperature and dose for samples used in these tests.

Table 1, *Listing of Materials Tested*

Ferritics	ODS/Nanoferritics
F82h-IEA	14CrYWT-H
MA956	14CrYWT-AR
T91	14CrYWT-UCSB-B
HT9	14CrYWT-UCSB-C
NF616	14CrYWT-ORNL
Eurofer	
97	MA957
CastSS	

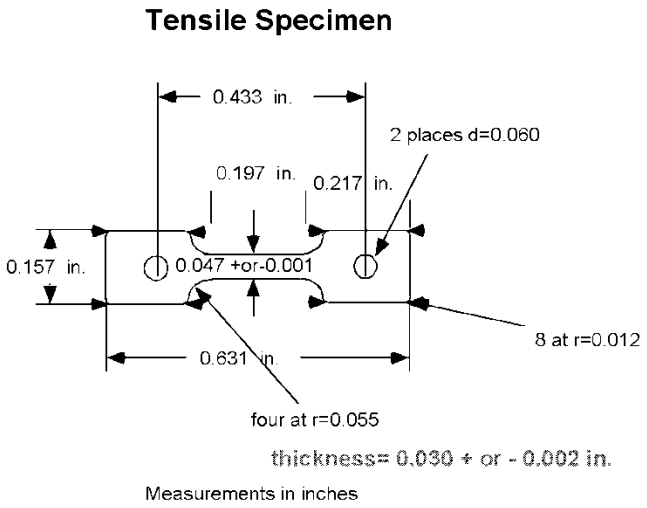

Figure 1, *Geometry of S-1 Tensile specimen, specimens from this irradiation were 0.020" thick and most did not have the holes in the center of the grip section.*

Table 2, Irradiation Temperature and Dose for samples from this irradiation

	Median Temp, C	DOSE, dpa	
Tensile	296.5	6.49	Most Tensiles
Tensile	293.5	4.36	MA956, 14YWT-H, 14YWT-Ar
DCT	285.5	4.94	Eurofer
DCT	272.5	6.04	F82, T91, HT9

Samples were cleaned in the hot cell corridor to remove alpha contamination that was picked up in the INL MFC hot cells. Samples were soaked in acetone to remove any fixative applied at INL, then placed in an MC3 (sodium metasilicate) ultrasonic bath, followed by an ultrasonic bath

in water and then an alcohol wash to dry the samples. Samples went through this procedure once or twice and resulted in all samples being measured NDA for removable alpha contamination.

Testing Conditions

Samples were tested on a 30 kN capacity Instron 5567 screw driven load frame located inside a hot cell in Wing 9 at the CMR facility at Los Alamos National Laboratory (Figure 2). The load frame is outfitted with an inert atmosphere furnace operable to 700 °C. Samples were loaded using manipulators into a set of ball end grips in an alignment fixture (Figure 3). Notably, a new shoulder loading fixture was used to test specimens that did not have holes drilled in the grip section (Figure 4). Tests were performed at a constant cross head velocity of 0.15 mm/minute corresponding to a nominal engineering strain rate of 5 $x10^{-4}$ /sec. Load/displacement data were converted to engineering stress/strain data using the initial measured specimen dimensions. The compliance from the test system was mathematically removed from each curve. Samples were tested at room temperature (reported previously) and at elevated temperatures corresponding to irradiation temperatures.

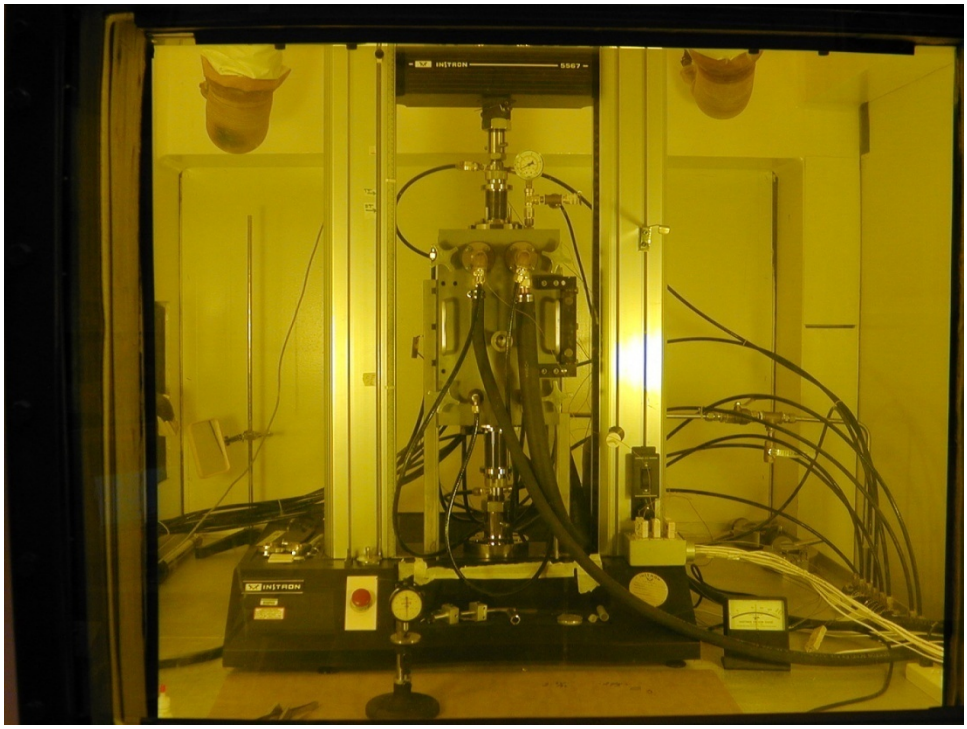

Figure 2 *Instron 5567 Load Frame, located in a hot cell at the CMR facility.*

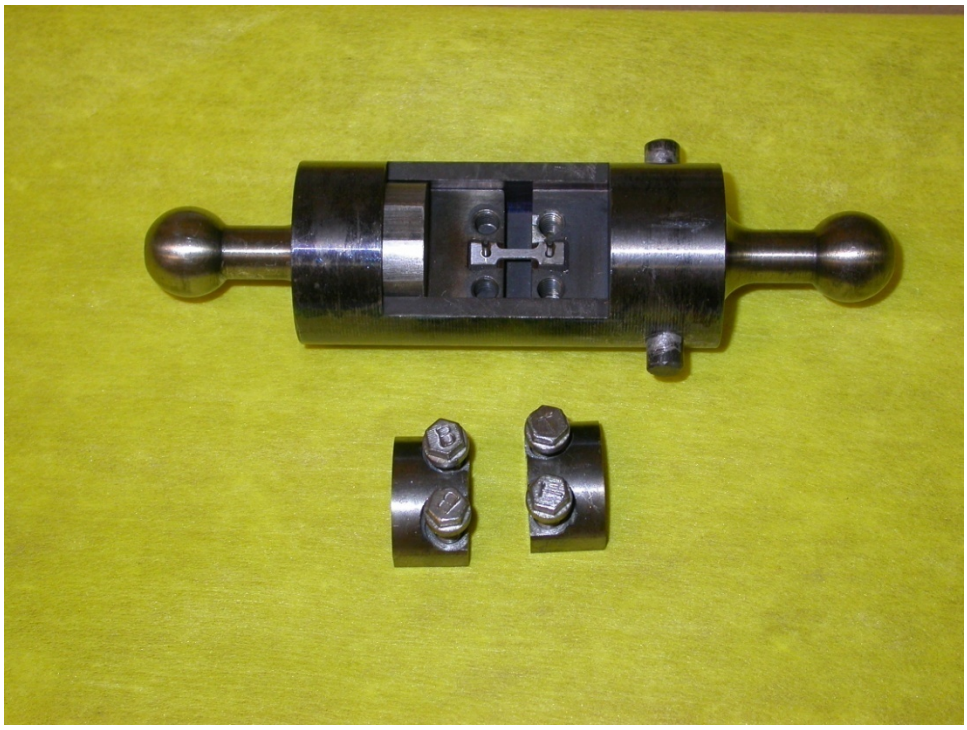

Figure 3 - *Ball end grips for samples with center hole.*

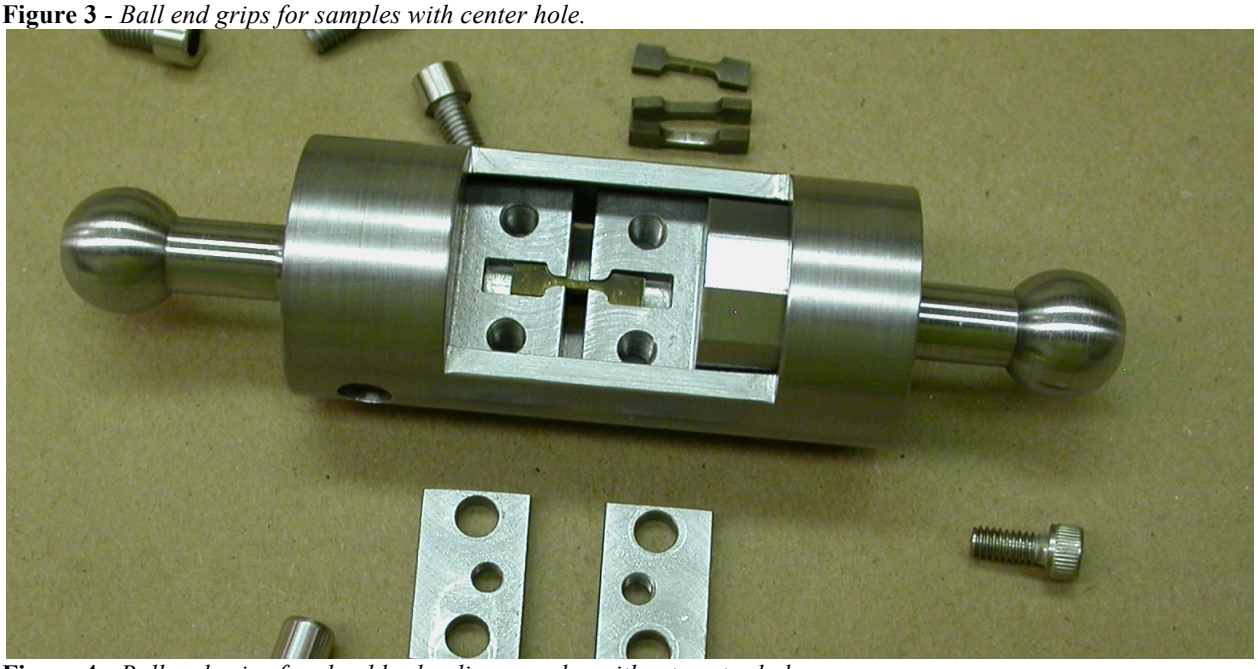

Figure 4 - *Ball end grips for shoulder loading samples without center hole.*

Tensile Results

The tables below display the Yield Strength, Ultimate Tensile Strength, Uniform Elongation and Total Elongation for control and irradiated samples tested at room temperature and 300°C. Table 3 displays the results for the ODS samples, while Table 4 displays the results of the Ferritic samples.

Table 3: Oxide Dispersion Strengthened Samples:

ODS NFA	ID	Type	Yield MPa	UTS MPa	Uniform Elongation %	Total Elongation %	temp
14CrYWT-Ar	CD24c	Control	815	1066	8.05	11.65	rt
	CD25c	Control	810	1062	5.1	6.65	rt
	CD26c	Control	745	989	5.84	8.6	rt
	CD27c	Control	755	1010	6.2	9	rt
	CD07	Irradiated	1175	1248	1.35	5.6	rt
	CD08	Irradiated	1180	1239	1.3	4.6	rt
	CD29c	Control	705	874	3.55	5.1	300c
	CD09	Irradiated	945	988	0.73	3.85	300c
14CrYWT-H	CC25c	Control	1045	1171	6.15	10.5	rt
	CC26C	Control	1045	1167	4.83	9.1	rt
	CC07	Irradiated	1185	1237	0.91	6.45	rt
	CC08	Irradiated	1230	1292	1.02	7.5	rt
	CC31c	Control	860	949	3.74	6.8	300c
	CC09	Irradiated	1000	1034.6	0.75	4.85	300c
14YWT-UCSB-B	YB#1c	Control	1015	1313	3.98	6.53	rt
	YB#2c	Control	1050	1314	3.57	5.5	rt
	YB06	Irradiated	795	795	0	0	rt
	YB07	Irradiated	1036	1036	0	0	rt
14YWT-UCSB-C	YC#1c	Control	955	1153	6.36	10.4	rt
	YC#2c	Control	955	1128	5.81	6.95	rt
	YC06	Irradiated	909	909	0	0	rt
	YC07	Irradiated	1097	1097	0	0	rt
14YWT-ORNL	CE09c	Control	1630	1805	0.93	4.35	rt
	CE10c	Control	1640	1847	0.86	4.7	rt
	CE07	Irradiated	1720	1856	1.24	3.72	rt
	CE08	Irradiated	1740	1867	1.12	3.3	rt
MA957	MA10c	Control	1030	1171	9.65	20.5	rt
	MA11c	Control	1035	1184	10.2	19.2	rt
	MA07	Irradiated	1230	1292	5.55	13.9	rt
	MA08	Irradiated	1260	1331	6.63	14.15	rt
	MA18c	Control	890	1002	6.05	16	300c
	MA09	Irradiated	1070	1104	3.65	12.05	300c

Table 4: Ferritic Samples

Ferritics	ID	Type	Yield MPa	UTS MPa	Uniform Elongation %	Total Elongation %	temp
HT9	TB#1c	Control	560	761	9.15	21	rt
	TB#2c	Control	550	753	9.7	21.4	rt
	TB01	Irradiated	1100	1175	4.54	10.9	rt
	TB02	Irradiated	1080	1151	3.53	7.75	rt
	TB#3c	Control	465	652	8.4	15.6	300c
	TB03	Irradiated	945	956	2.45	7.63	300C
T91	TA#1c	Control	610	734	7.28	17.45	rt
	TA#2c	Control	610	726	6.32	16.38	rt
	TA04	Irradiated	1055	1102	1.07	5.7	rt
	TA05	Irradiated	1005	1078	0.9	3.8	rt
	TA#3c	Control	453	596	4.83	12.9	300c
	TA06	Irradiated	880	939	1.51	5.85	300c
Eurofer 97	ER07c	Control	540	656	6.77	21.35	rt
	ER08c	Control	515	646	7.05	19.3	rt
	ER04	Irradiated	945	979	0.69	7.1	rt
	ER05	Irradiated	905	950	0.72	5.5	rt
	ER#1c	Control	425	510.11	3	12.5	300c
	ER06	Irradiated	725	832	2.18	4.2	300c
F82H-IEA	HA14c	Control	519	625	5.34	17.5	rt
	HA15c	Control	523	629	5.31	17.1	rt
	HA04	Irradiated	849	929	0.59	5.58	rt
	HA05	Irradiated	927	984	0.61	5	rt
	HA16c	Control	450	522	2.81	12.7	300c
	HA07	Irradiated	802	819	0.51	5.9	300c
NF616	NF07c	Control	740	863	4.83	13.35	rt
	NF08c	Control	730	857	5.96	14	rt
	NF04	Irradiated	1120	1154	0.65	4.7	rt
	NF05	Irradiated	1100	1133	0.57	3.9	rt
	NF09c	Control	630	718.7	3.34	9.1	300c
	NF06	Irradiated	960	1003.5	0.68	2.75	300c
MA956	MB#1c	Control	690	760	9.45	14.8	rt
	MB#2c	Control	690	766	8.72	12.6	rt
	MB06	Irradiated	1065	1067	0.23	0.75	rt
	MB07	Irradiated	1080	1081	0.21	1.05	rt
	MB#3c	Control	573	680	8.7	10.25	300c
	MB08	Irradiated	864	865.7	0.17	2.9	300c
CastSS	CS12c	Control	259	470	43.1	53.1	rt
	CS04	Irradiated	783	789	0.3	10.7	rt
	CS05	Irradiated	823	824	0.32	9.8	rt
	CS09c	Control	130	327	50.5	53.5	300c
	CS07	Irradiated	605	607.6	0.18	6.8	300c

Figure 5 shows the stress-strain curves of the three lots of ODS samples tested at 300°C. As with the room temperature tests, the MA957 displays notable ductility in the irradiated state.

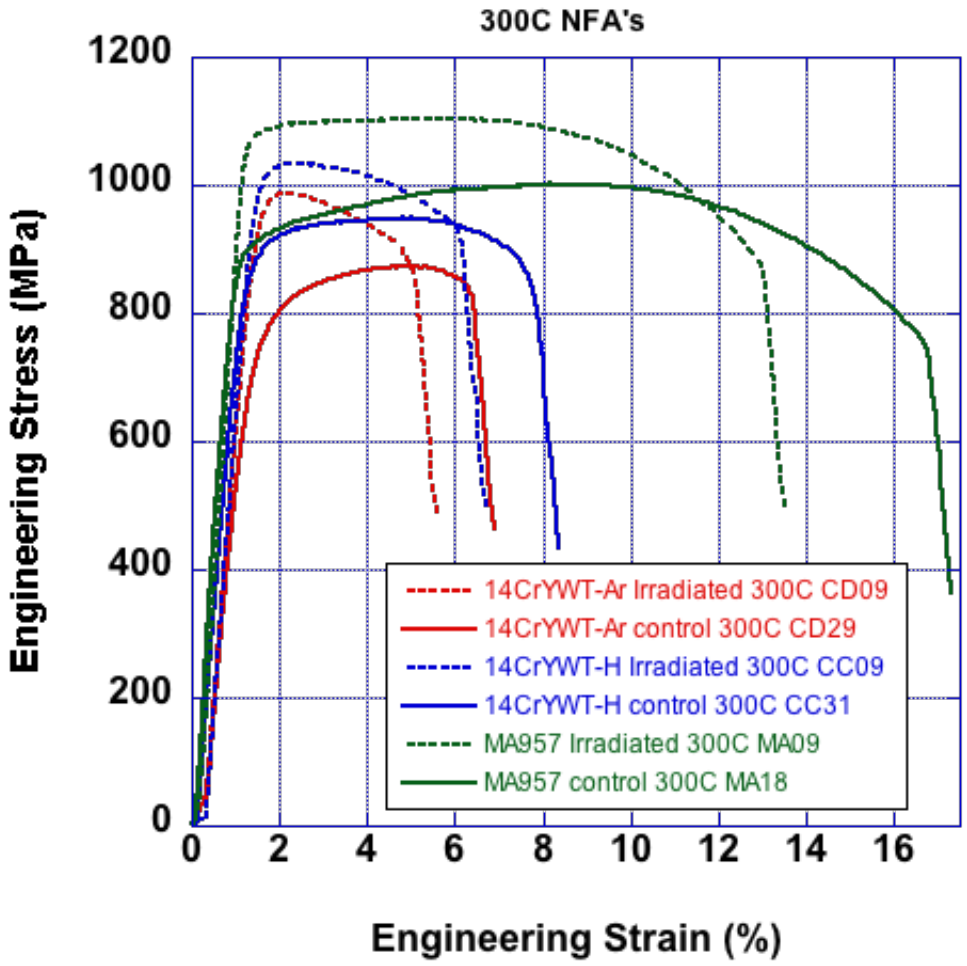

Figure 5*: Engineering stress strain curves for ODS samples tested at 300°C.*

Figure 6 shows the engineering stress strain curves for all the ferritic samples tested at 300°C. Figure 7 shows only the most ductile samples from this lot, HT-9, T91 and EuroFer97. As with the room temperature experiments, HT-9 displays the best ductility when tested at 300°C.

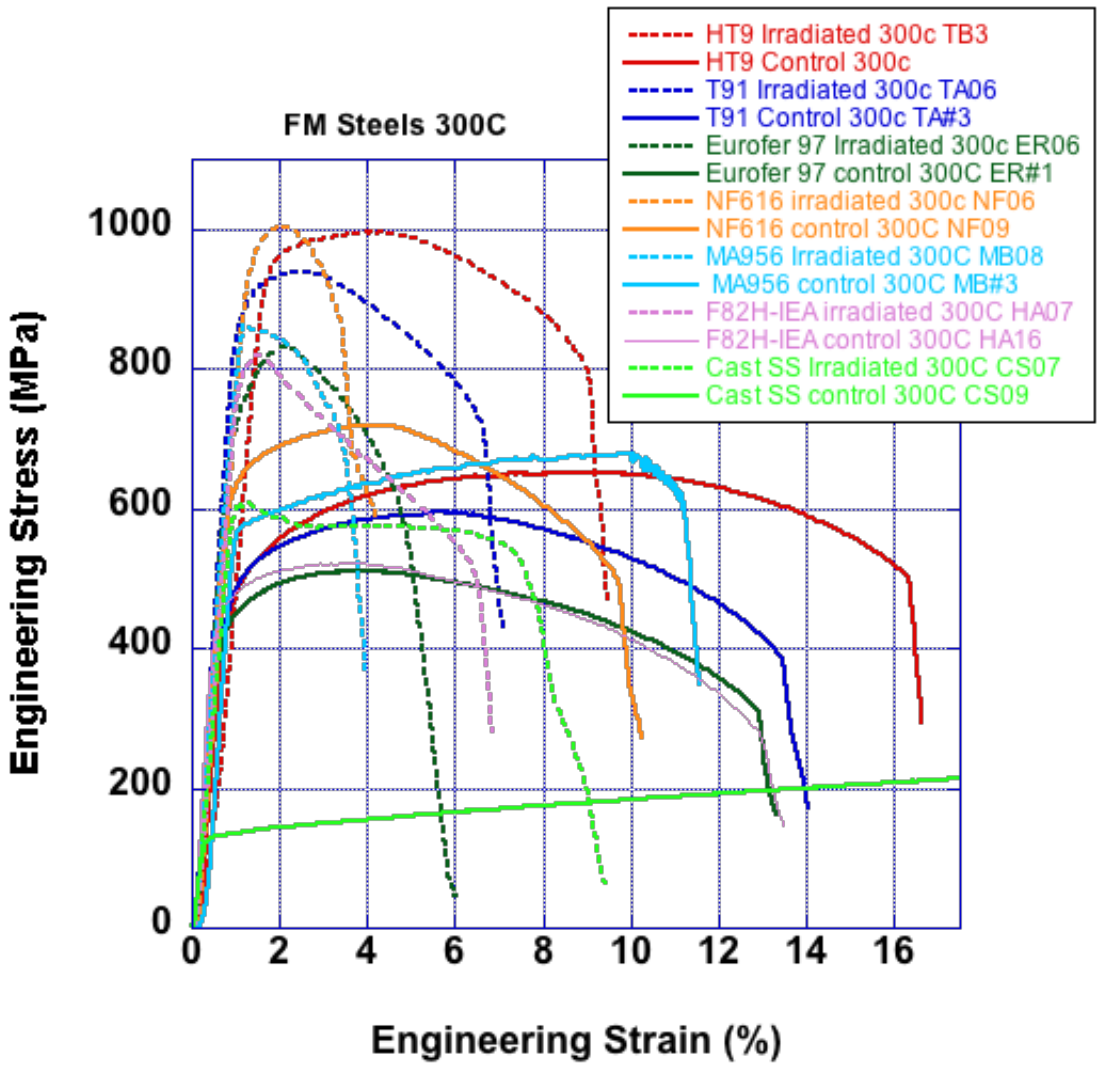

Figure 6*: Engineering stress strain curves for all ferritic samples tested at 300°C.*

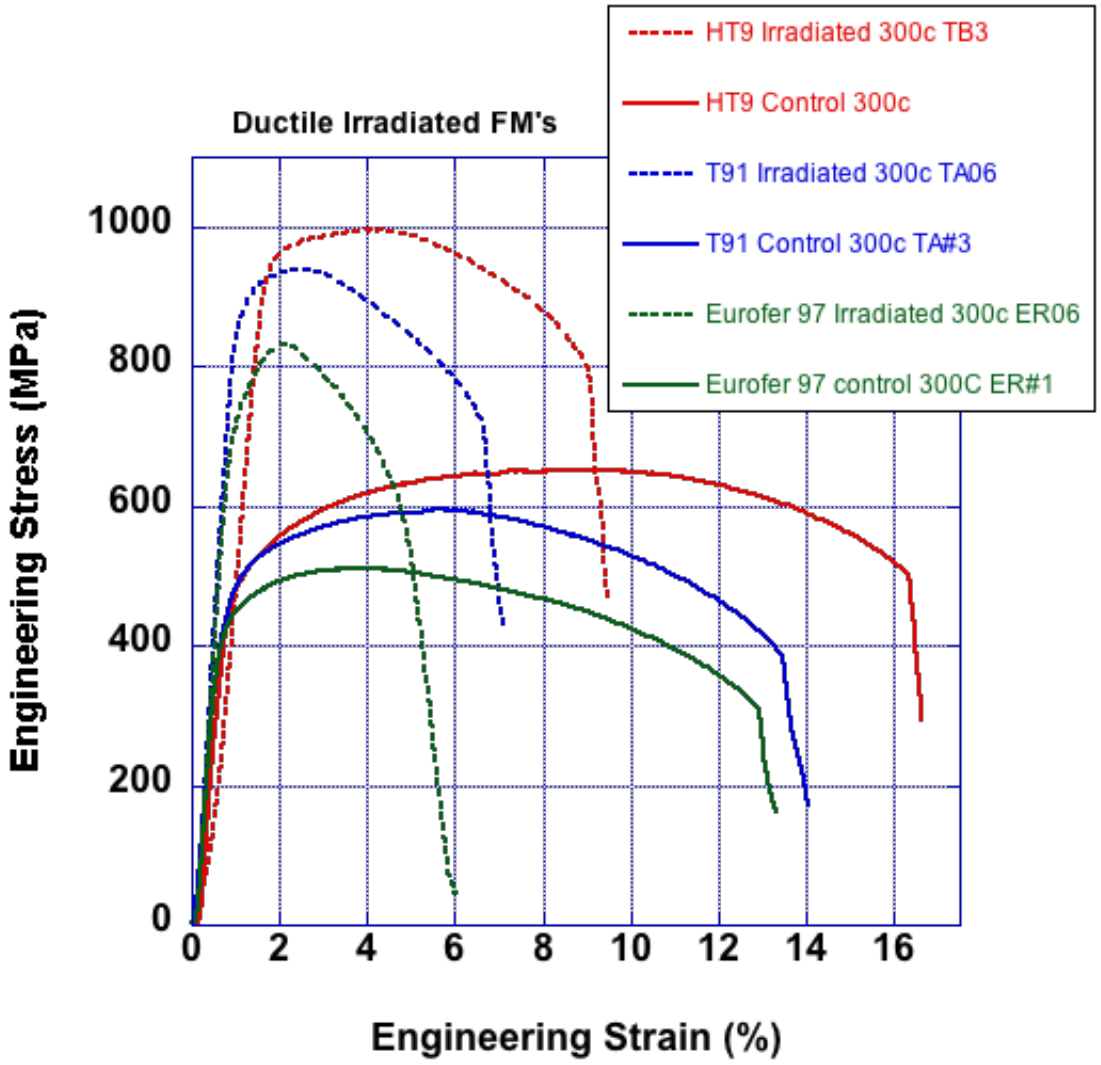

Figure 7*: Engineering stress strain curves for the most ductile ferritic samples tested at 300°C: HT-9, T91, and EuroFer97.*

Reduction in Area Calculation

Reduction in area was calculated for the most ductile samples tested at room temperature. The fracture cross section of samples was measured using the HIROX digital optical microscope located in the hot cell. As received initial dimensions were measured using a dial micrometer prior to the tensile tests. Profile images were used to measure the reduction in area in cases where the samples did not fracture during the tests. The reduction in area correlates as expected with the elongation measured in the tensile tests. Most samples that fractured revealed a relatively even and ductile appearing microstructure, an example is seen in Figure 8a, the cross section of the irradiated HT-9 sample. MA957 did display extensive cracking on the fracture surface, although the sample did also display the largest reduction in area of the all the irradiated samples and the largest uniform and total elongation during the tensile tests (Figure 8b). The control HT-9 sample, irradiated NF616 and irradiated EuroFer97 samples did not fracture during testing. Table 5 shows the reduction in area calculations compared to the room temperature mechanical property data. All cross section images can be found in Appendix B.

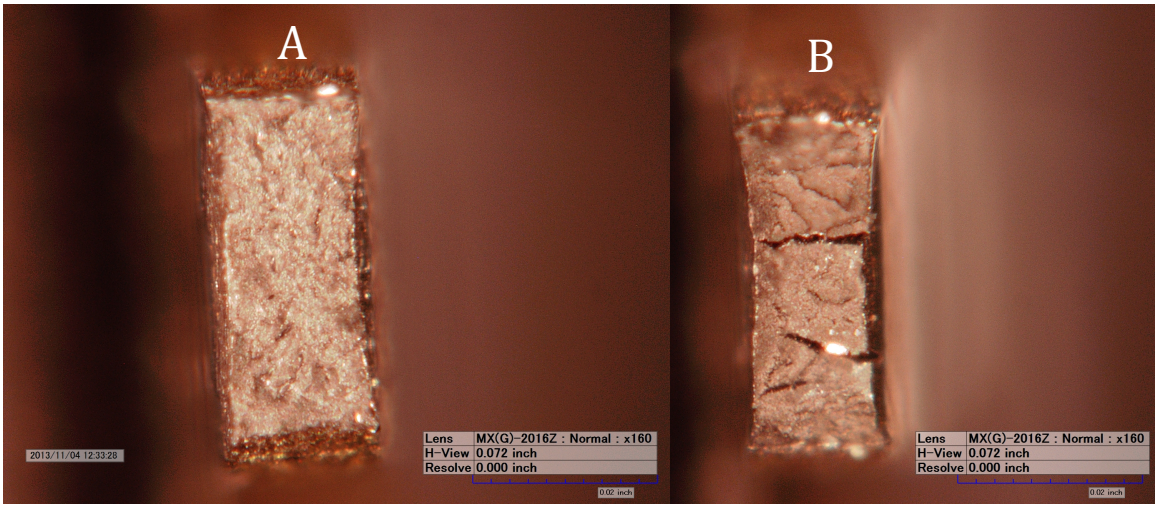

Figure 8: *Fracture surface of irradiated HT-9 (A) and MA957 (B)*

Table 5: Reduction in area and mechanical testing data for the more ductile samples tested at room temperature from the ATR irradiation.

Material	ID	Type	Yield MPa	UTS MPa	Uniform Elongation %	Total Elongation %	Reduction in Area %
HT9	TB#1c	Control	560	761	9.15	21	55.03
HT9	TB01	Irradiated	1100	1175	4.54	10.9	46.22
T91	TA04	Irradiated	1055	1102	1.07	5.7	39.03
NF616	NF04	Irradiated	1120	1154	0.65	4.7	23.72
MA957	MA08	Irradiated	1260	1331	6.63	14.15	50.38
F82H-IEA	HA05	Irradiated	927	984	0.61	5	25.87
Eurofer 97	ER04	Irradiated	945	979	0.69	7.1	39.18
14YWT-ORNL	CE08	Irradiated	1740	1867	1.12	3.3	25.90
14CrYWT-Ar	CD07	Irradiated	1175	1248	1.35	5.6	28.45
14CrYWT-H	CC07	Irradiated	1185	1237	0.91	6.45	40.53

Synchrotron Experiments.

Small samples (~1x1mm in cross section) were cut from the undeformed grip section of 4 different irradiated samples and were shipped to Brookhaven National Labs for experiments on the NSLS Synchrotron. Numerous control samples for these alloys and other ATF claddings were sent for measurement, and some HT-9 control and irradiated specimens from the ACO-3 lot were measured as well. Pair Distribution Function (PDF), High Resolution X-Ray Diffraction (HRXRD) and Small Angle X-Ray Scattering (SAXS) experiments were performed. Table 6 lists the irradiated samples from the UCSB-NSUF irradiation that were measured.

Table 6: Irradiated samples sent to BNL for PDF, HRXRD and SAXS

Sample ID	Material	Dose at 30cm	Dose at contact
CE07	14YWT-ORNL	70 mR/hr	3.9 R/hr
MA08	MA957	15 mR/hr	1 R/hr
TA04	T91	27 mR/hr	1.5 R/hr
TB01	HT-9	6 mR/hr	250 mR/hr

What follows is the initial analyses of data taken. Small volume fraction second phase information is still being analyzed. Ongoing confirmatory microscopy will help settle the volume fractions and phases.

High-resolution x-ray diffraction (XRD), small angle x-ray scattering (SAXS) and atomic pair-distribution function (PDF) measurements were performed at the NSLS, using the high-energy x-rays available at beamlines X17A. Figure 9 shows a schematic of the beamline at X17A with all optical and detector elements labeled for reference. For both sets of measurements an a-Si pixel array detector (2048x2048 pixels) was mounted orthogonal to the beam path, centered on the beam.

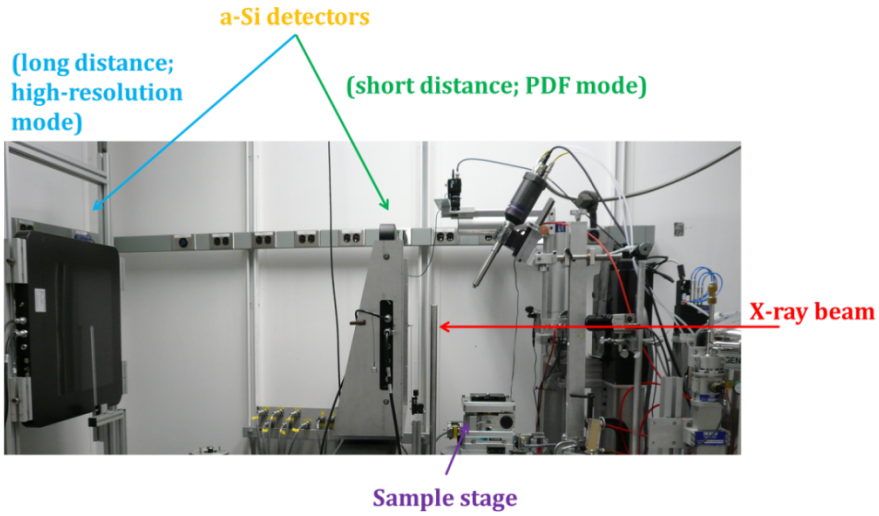

Figure 9. Photo of X17A endstation at the NSLS.

The sample-to-detector distance and tilt of the detector relative to the beam were refined using a Nickel NIST powder standard. At X17A the wavelength of the incident x-rays is 0.1839 (67.42 keV). The sample-to-detector distances (SDD's) were calculated to be ~200 mm and ~1560 at the near and far detectors, respectively. The larger SDD (with smaller scattering vector, Q) was used for the SAXS and Rietveld analysis of the XRD patterns, while the short distance was used for the PDF analysis (wider Q-space). Multiple patterns were collected on 2-3 different regions of each sample with count times adjusted to the maximize signal and to be away from the saturation limit of the detector. Typical count times were 0.5-1 sec (depending on the sample), and each image consisted of 100 individual exposures (to maximize signal to noise ratio). All raw .tiff images were background corrected by subtracting a dark current image (collected at an identical rate without exposing the detector to x-rays) and masking regions of the images with noticeable artifacts (beam stop, shadowing and edge of the detector). The corrected two-dimensional images were then averaged together and radially integrated, excluding the area in which the beamstop arm shadowed the scattered beam, to obtain the one-dimensional powder diffraction pattern.

Results:

F/M (ACO-3 duct)

All samples, with the exception of PM2000 and MA957, showed powder-like patterns with no obvious preferred orientation. Figure 10 shows the two-dimensional detector patterns for the nano-ferritic alloys PM2000 and MA957 samples. The PM2000 sample shows a strong preferred orientation and MA957 shows a "spotty" XRD pattern. Figure 11 shows the reduced diffraction patterns for the standards and irradiated samples. The primary phases in these samples are the Ferrite (HT9-ACO, T91, HT9-QA) and Austenite (FCC Fe in the MA957 and HA457), and the $M_{23}C_6$ carbide.

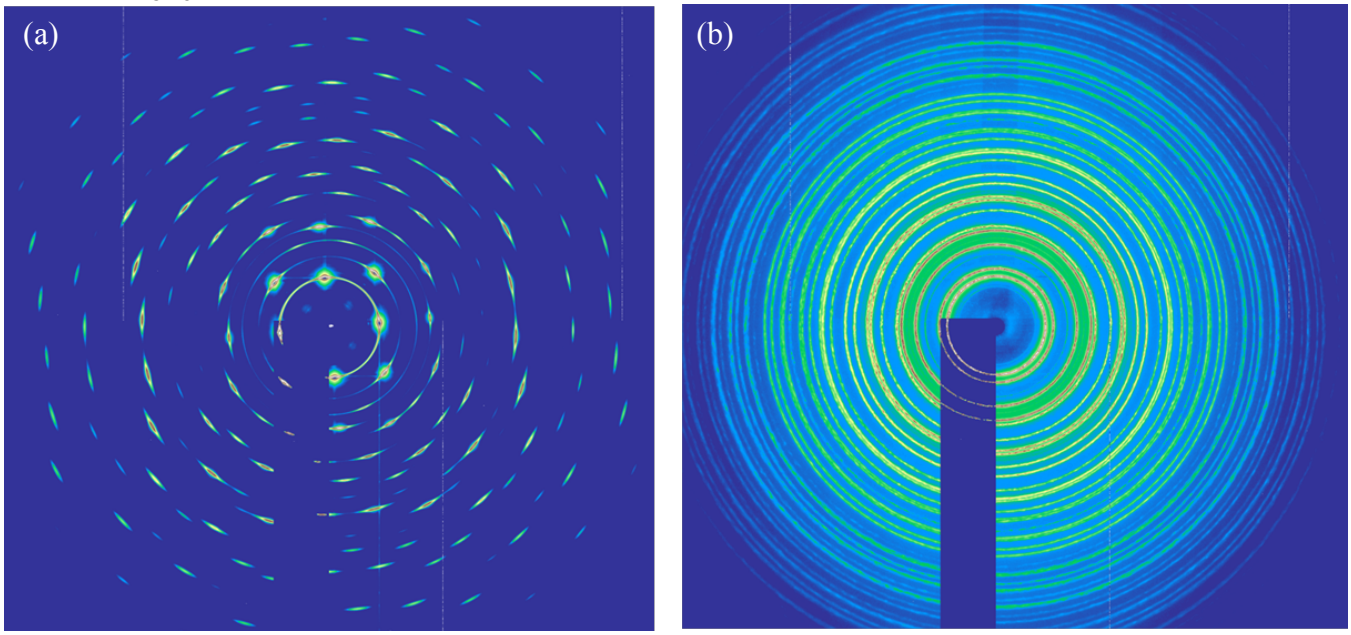

Figure 10.Two dimensional detector images of (a) PM2000 and (b) MA957 samples.

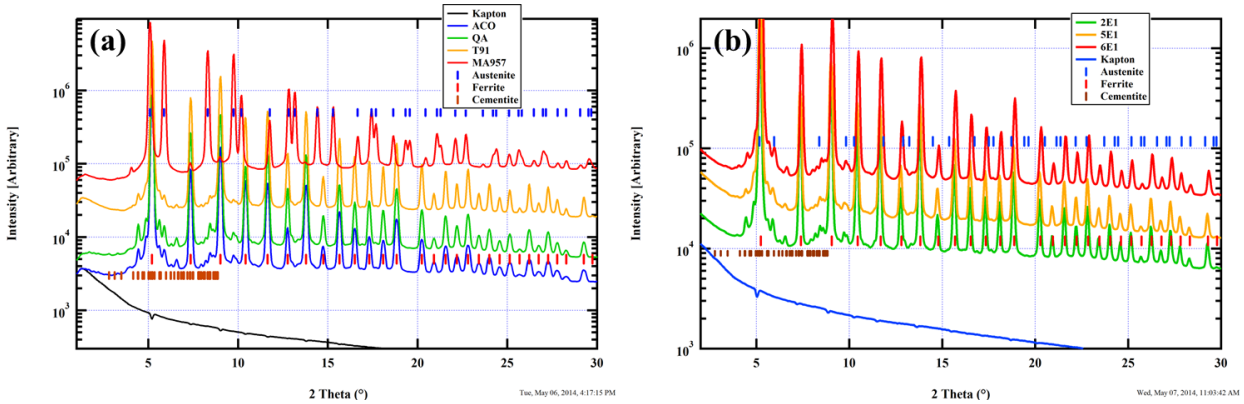

Figure 11.XRD patterns for (a) standards and (b) irradiated samples. The phases of the peaks are also labelled and the Kapton background is included for reference.

Figure 12 shows the background subtracted SAXS patterns for the unirradiated and irradiated samples. Differences in the SAXS patterns are observable across all samples. The MA957 and PM2000 samples have the highest scattering intensities, due to the oxide nanoparticles. The irradiated samples provided also show visible changes in the SAXS patterns, with an increasing scattering from samples with higher dose. This increase in the scattering has previously been attributable to voids and the precipitation of alloy elements in the ACO duct samples [1].

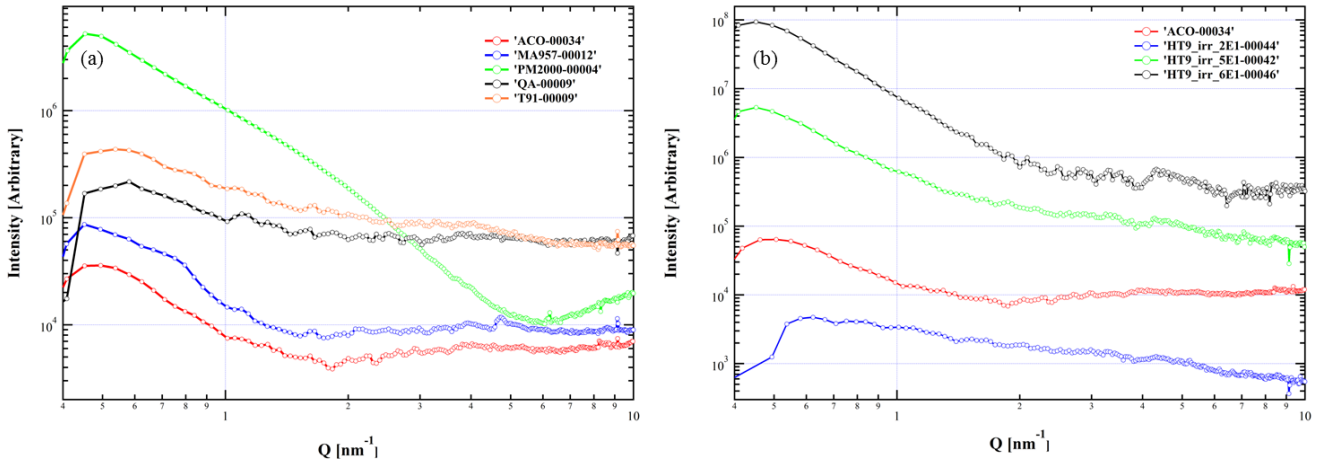

Figure 12. background corrected SAXS patterns for the (a) FM standards and (b) ACO irradiated samples.

MA957/14YWT/HT9/T91

SAXS/XRD and PDF measurements were made on all samples. Table 1 summarizes the samples that showed texture in their diffraction patterns. Figure 13 shows the reduced SAXS patterns for each of the four different control and irradiated samples. Large SAXS signals are readily visible for all unirradiated samples, with broad tails extending to high-*Q*. This is a common signature of a particle distribution and/or multiple distributions. Significant changes are also observed after irradiation in all samples, with the apparent removal of the high-*Q* scattering and changes in the SAXS intensity and shape[1].

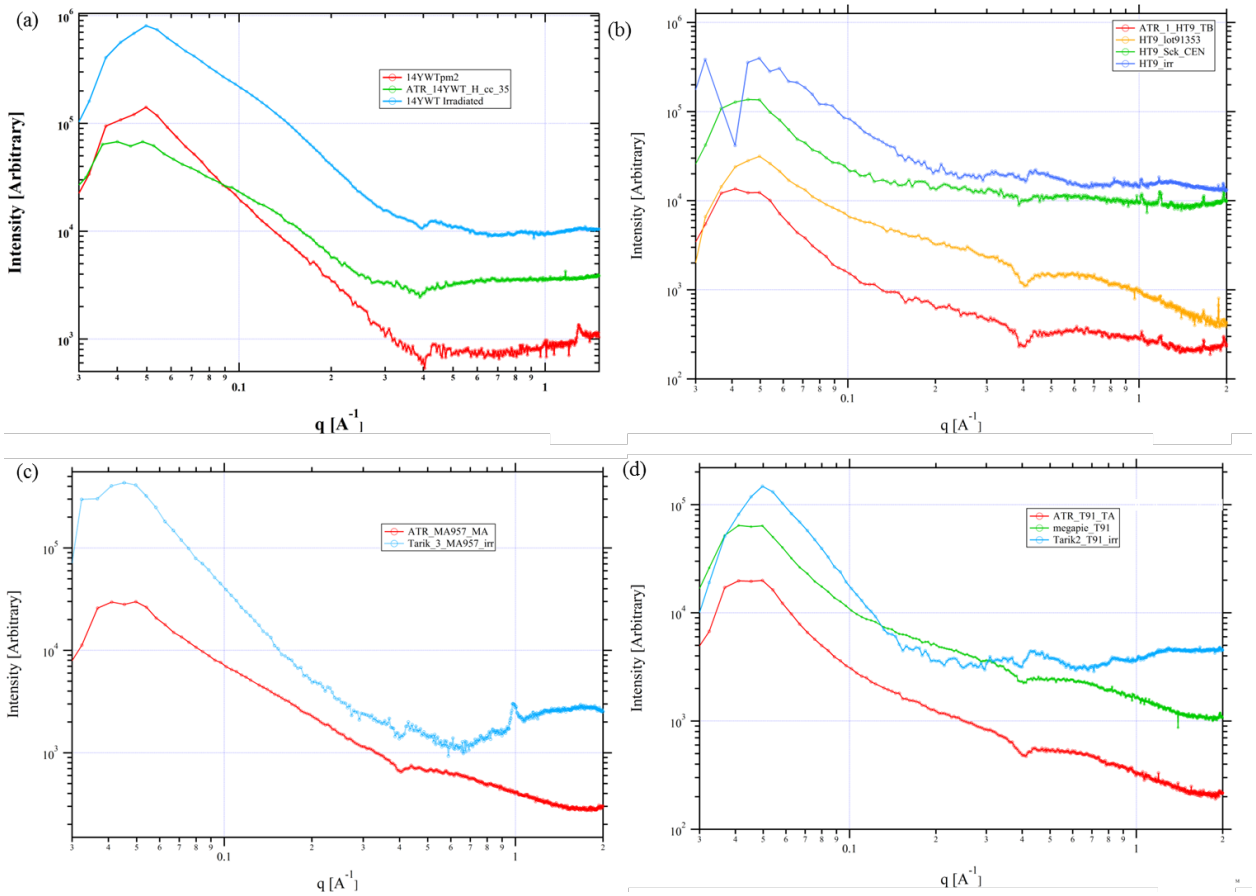

Figure 13 Background corrected SAXS (air and Kapton scatter removed) patterns for the (a) T91, (b) HT9, (c) 14YWT and (d) MA-957 samples.

Figure 14 shows the XRD patterns for all samples with the identified phases included for reference. All unirradiated T91 samples showed an Austenite, Ferrite and an $M_{23}C_6$ component. The positions of the pure $Cr_{23}C_6$ phase taken from the literature [2], however, do not match up with the measured peak positions. The peaks for the ternary $Cr_{21}Fe_2C_6$ phase [3], with a contracted unit cell, are much closer to the measured data as is more clearly shown in Figure 14 (a). After

[1] The negative peak at ~0.4 Å^{-1} is due to the use of a Kapton background, dissimilar to the Kapton used to contain the samples.

irradiation, the Ferrite peaks shift slightly to lower two-theta (indicating that the lattice has expanded). Furthermore, a small Austenite component is retained after irradiation and the $M_{23}C_6$ peaks have decreased in intensity.

The unirradiated HT9 samples show evidence of a three-phase system, with a smaller volume fraction of Austenite, compared to T91. There are visible microstructural differences in the all three identified phases in the control samples, potentially the result of different size/strain and volume fraction (preliminary quantitative analysis confirms this). After irradiation, various structural changes ensue and qualitatively include the removal of the Austenite phase while the $M_{23}C_6$ peaks appear to be unchanged. A larger background was also measured in the irradiated samples, potentially indicative of a radiation-induced formation of a disordered phase.

The unirradiated 14YWT samples show evidence of an extra phase that is different from the $M_{23}C_6$ phase; possibly attributable to the small nanoparticles introduced during casting (YTO oxide nanoprecipitates). Like the HT9 samples, irradiation leads to the removal of the peaks associated with the Austenite and nanoparticle phase. The $M_{23}C_6$ precipitates may also be increasing in volume fraction (or size) after irradiation, with higher intensity and slightly sharper peaks.

Like the 14WYT sample, the MA957 sample shows a small Austenite component, $M_{23}C_6$ and an unidentified component at $\sim$2.5 $Å^{-1}$ (potentially attributable to the nanoparticles introduced during the casting process). After irradiation, all peaks corresponding to the secondary phases disappear and are replaced by a less defined broad peaks and an increase in the background. This may be indicative of a crystalline-to-amorphous phase transformation.

Finally, additional (broad) minor peaks are also observable across all irradiated samples that have yet to be completely identified (potentially G-phase or Cr rich α' precipitates).

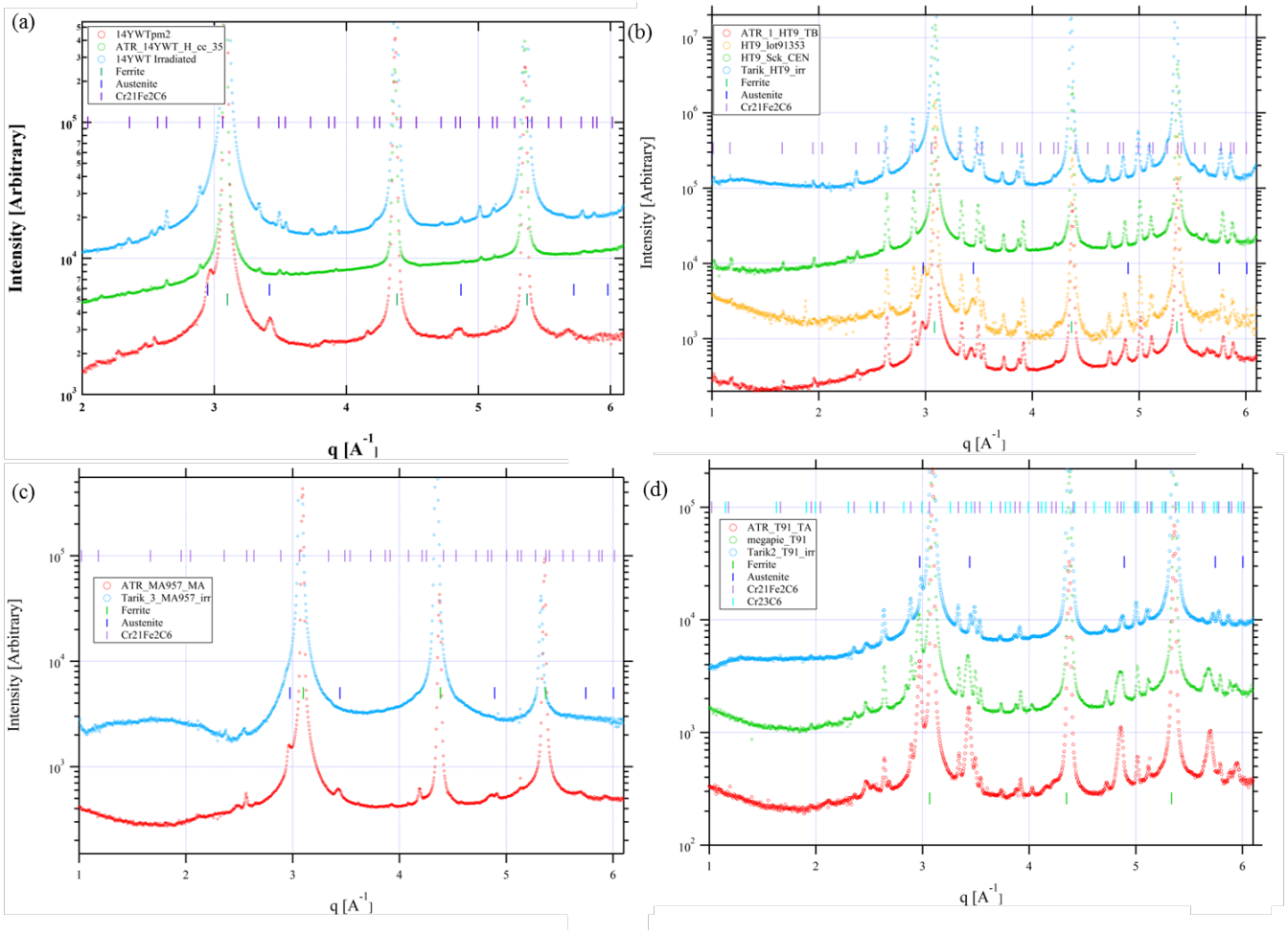

Figure 14. Background subtracted (kapton and air scatter) reduced one dimensional XRD patterns for the (a) 14YWT, (b) HT9, (c) MA-957 and (d) T91 samples. The identified phases are included for reference

Figure 15 shows the reduced PDF for all samples measured. Quantitative PDF analysis in the samples that have significant texture is problematic and difficult due to the necessity of complete Debye-rings, but may be useful in observing changes qualitatively in the local atomic structure (14YWT, MA957). The HT9 and T91 samples that did not show texture, do show changes in the local atomic structure, with the Fe matrix peaks decreasing with irradiation, potentially due to an increase in the structural disorder.

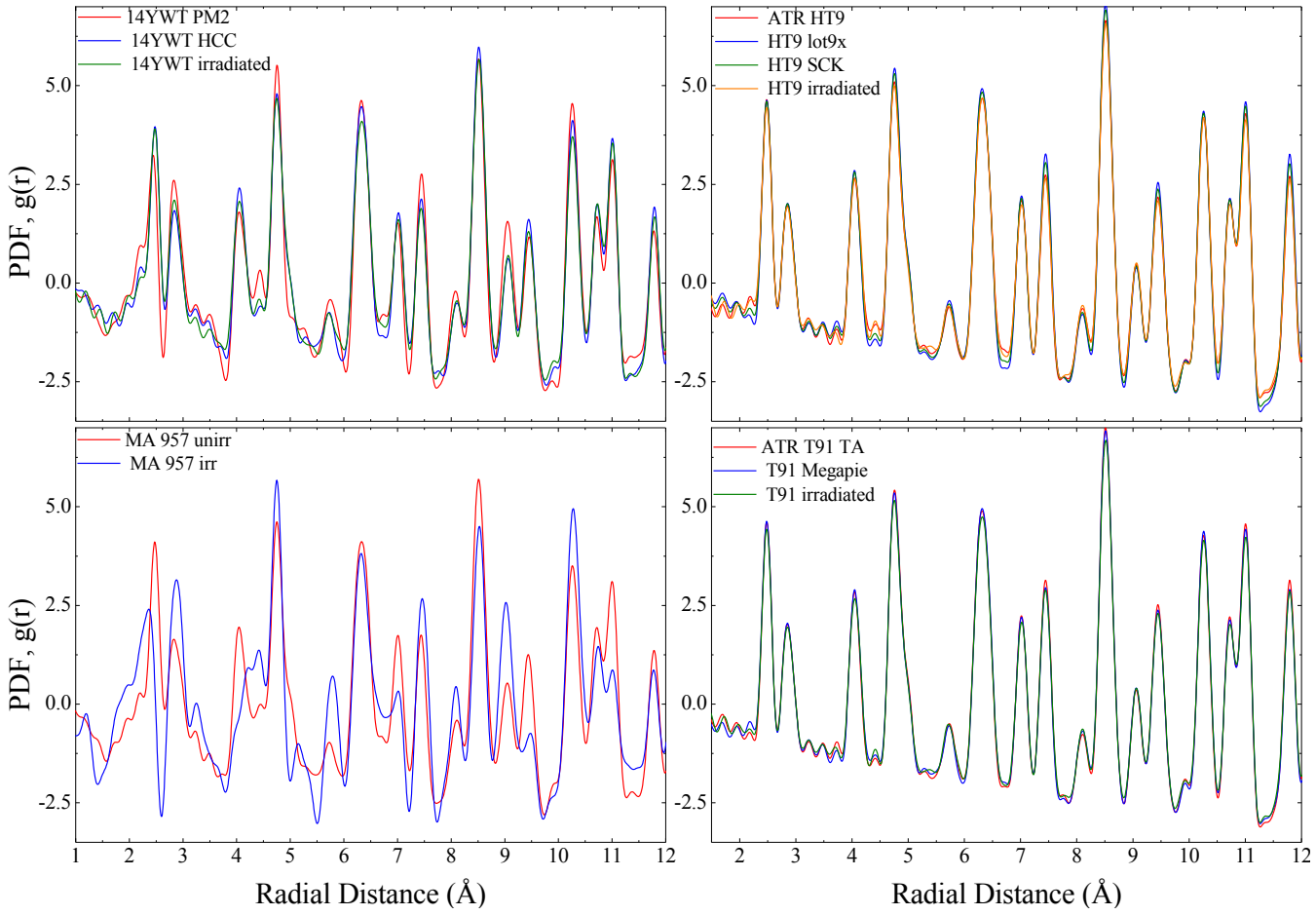

Figure 15. PDFs for the for the (a) 14YWT, (b) HT9, (c) MA-957 and (d) T91 samples.

Table 7. XRD and PDF patterns that show texture

Sample	Texture XRD	Texture PDF
HT9 lot 91353	no	no
HT9 SCK-CEN	no	no
ATR-1 HT9 "TB"	weak	no
Megapie T91	no	no
ATR T91-TA	no	no
ATR-MA957 MA	yes (strong)	yes (strong)
ATR-14YWT-H "CC 35"	weak	weak
14YWT-PM2	yes (strong)	yes (strong)
HT9 irradiated 1 (14YWT_ORNL)	yes (weak)	yes (weak)
HT9 irradiated 2 (T91)	no	no
HT9 irradiated 3 (MA957)	yes (strong)	yes (strong)
HT9 irradiated 4 (HT9)	no	no

References:

[1] P. L. Mosbrucker, D. W. Brown, O. Anderoglu, L. Balogh, S. A. Maloy, T. A. Sisneros, J. Almer, E. F. Tulk, W. Morgenroth, and A. C. Dippel, J. Nucl. Mater. 443, 522 (2013).

[2] Xie J., Shen J., Chen N., Seetharaman S.: "Site preference and mechanical properties of Cr23-xTxC6 and Fe21T2C6 (T= Mo, W)", Acta Mater. 54 (2006) 4653.

[3] Yakel H.L.: "Atom Distributions in Tau-Carbide Phases: Fe and Cr Distributions in (Cr23-xFex)C6 with x= 0, 0.74,1.70,4.13, and 7.36", Acta Crystallogr. B 43 (1987) 230.

Appendix A

		ID	Material
Packet 9-4	1	HA8	F82H-IEA
	2	HA9	F82H-IEA
	3	HA10	F82H-IEA
	4	HA11	F82H-IEA
	5	HA12	F82H-IEA
	6	HA13	F82H-IEA
	7	MB6	MA956
	8	MB7	MA956
	9	MB8	MA956
	10	MB9	MA956
	11	CC7	14CrYWT-H
	12	CC8	14CrYWT-H
	13	CC9	14CrYWT-H
	14	CC10	14CrYWT-H
	15	CD7	14CrYWT-AR
	16	CD8	14CrYWT-AR
	17	CD9	14CrYWT-AR
	18	CD10	14CrYWT-AR

		ID	Material
Packet 7-3	1	TA4	T91
	2	TA5	T91
	3	TA6	T91
	4	Tb1	HT9
	5	TB2	HT9
	6	TB3	HT9
	7	NF4	NF616
	8	NF5	NF616
	9	NF6	NF616
	10	HA17	F82H-IEA
	11	HA4	F82H-IEA
	12	HA5	F82H-IEA
	13	HA6	F82H-IEA
	14	HA7	F82H-IEA
	15	HA18	F82H-IEA
	16	HA19	F82H-IEA
	17	HA20	F82H-IEA
	18	HA21	F82H-IEA
	19	HA22	F82H-IEA
	20	ER4	Eurofer 97
	21	ER5	Eurofer 97
	22	ER6	Eurofer 97
	23	MA7	MA957
	24	MA8	MA957
	25	MA9	MA957
	26	YB6	14YWT-UCSB-B
	27	YB7	14YWT-UCSB-B
	28	YB8	14YWT-UCSB-B
	29	YC6	14YWT-UCSB-C
	30	YC7	14YWT-UCSB-C
	31	YC8	14YWT-UCSB-C
	32	CE(x)7	14YWT-ORNL
	33	CE(x)8	14YWT-ORNL
	34	CS4	Cast SS
	35	CS5	Cast SS
	36	CS7	Cast SS

Controls

HT9 (TB)……...0 specimens
NF616 (NF)…….....12 specimens
T91 (TA)…….....2 specimens
F82H-IEA (HA)……..11 specimens (unmodified gage section)
F82H-IEA (HA)……....4 specimens (offset notched gage section)
F82H-IEA (HA)……1 specimen (centered notched gage section)
F82H-IEA (HA)……0 specimens (center hole gage section)
Eurofer97 (ER)……..2 specimens
MA957 (MA)……..10 specimens
MA956 (MB)…….....6 specimens
14CrYWT UCSB B (1000°C) (YB)….3 specimens
14CrYWT UCSB C (1150°C) (YC)….2 specimens
Cast Stainless Steel (CS)……....7 specimens
14CrYWT -H (CC)……..11 specimens
14CrYWT-Ar (CD)……13 specimens
14CrYWT –ORNL (CE)……...2 specimens

Ferritics	ODS/Nanoferritics
F82h-IEA	14CrYWT-H
MA956	14CrYWT-AR
T91	14CrYWT-UCSB-B
HT9	14CrYWT-UCSB-C
NF616	14CrYWT-ORNL
Eurofer 97	MA957
CastSS	